iJRASET
International Journal For Research in Applied Science and Engineering Technology

INTERNATIONAL JOURNAL FOR RESEARCH

IN APPLIED SCIENCE & ENGINEERING TECHNOLOGY

Volume: 13 **Issue:** VIII **Month of publication:** August 2025

DOI: https://doi.org/10.22214/ijraset.2025.73634

www.ijraset.com

Call: 08813907089 | E-mail ID: ijraset@gmail.com

International Journal for Research in Applied Science & Engineering Technology (IJRASET)
ISSN: 2321-9653; IC Value: 45.98; SJ Impact Factor: 7.538
Volume 13 Issue VIII Aug 2025- Available at www.ijraset.com

Assessment of Radioelements Host Potential Using Geophysical Methods in Gaya and Its Environs, Northwestern, Nigeria

Babagana A. Mustapha[1], Mohammad Saleh[2], Umar Suleiman[3], Abba Kaka A.Modu[4] , Maikori Bitrus Buba[5], Yakubu Ayuba Alak[6], Saidu Fika Ibrahim[7], Dashe Sylvia Tapsak[8]
[1, 2, 4] *Department of Physics, Faculty of Physical Sciences, Bayero University Kano, Nigeria*
[3, 5,6,7,8] *National Centre for Remote Sensing Jos, Nigeriaa*

Abstract: ***Radioactive mineral occurrences in Gaya and its environs, Northwestern Nigeria, have not been extensively studied using integrated airborne geophysical methods. This study aimed to delineate the Structural controls and assess the distribution of radioelements in the area to support mineral exploration and environmental safety evaluation. High-resolution aeromagnetic and aeroradiometric datasets (Sheet No. 82) from the Nigerian Geological Survey Agency were processed using Oasis Montaj and ArcGIS software. Data enhancement techniques included reduction to pole, analytical signal, first vertical derivative, source parameter imaging, ternary radiometric mapping, and dose rate estimation. Residual magnetic anomalies ranged from −293.2 to 436.1 nT, with depth estimates indicating shallow sources (0.08–0.20 km) and deeper sources (0.26–0.80 km). Mean concentrations of potassium, equivalent uranium, and equivalent thorium were 0.70 %, 2.79 ppm, and 12.13 ppm respectively, with high-value zones aligning with NE–SW and NW–SE structural trends. Absorbed dose rates ranged from 0.97 to 464.33 nGy h^{-1}, averaging 47.09 nGy h^{-1}, which is well below IAEA and UNSCEAR safety thresholds. The findings confirm that mineralization is structurally controlled and provide a geophysical framework for targeted exploration, environmental monitoring, and sustainable resource development in the region.***

Keywords: Aeromagnetic, Aeroradiometric, Radioelement Dose Rate, Exposure rate

I. INTRODUCTION

Nigeria is endowed with a diverse range of solid mineral resources distributed across its states. According to the Nigerian Geological Survey Agency (NGSA, 2023), about 34 significant mineral deposits occur across the country, offering vast opportunities for economic diversification and investment. Among these, radioactive minerals such as uranium and thorium are of particular interest due to their strategic industrial and energy applications.

In the civilian sector, uranium serves as a crucial fuel for nuclear power generation. Its fissile isotope, 235U, can be enriched to sustain controlled chain reactions for electricity production (Lenntech, 2023). Another isotope, 238U, is widely used in radiometric dating to determine the age of rocks (Lenntech, 2023). Thorium, valued for its alloying properties, improves the strength and high-temperature resistance of materials and is considered a potential alternative nuclear fuel. It is about three times more abundant than uranium and nearly four times more abundant than lead, with a higher potential energy yield than uranium or fossil fuels (UMMC, 2013). Potassium, while primarily recognized as an essential nutrient for biological systems, is also a measurable radioelement in geophysical surveys (UMMC, 2013). On average, uranium and thorium occur at concentrations of about 2.8 ppm and 10 ppm, respectively, with a typical thorium-to-uranium (Th/U) ratio in most rocks ranging from 1 to 3.5 (Plant et al., 2003).

Airborne magnetic and radiometric geophysical surveys provide a cost-effective means of assessing large and often inaccessible regions for mineral exploration and geological mapping. Magnetic surveys are effective in detecting structural features such as faults, contacts, joints, and basement configurations, as well as estimating the depth to the magnetic basement, geothermal gradients, and identifying favorable zones for ore or hydrocarbon accumulation (Eldosouky et al., 2017; Elkhateeb & Abdellatif, 2018). Gamma-ray spectrometry, on the other hand, measures the surface distribution of naturally occurring radioelements—thorium (eTh), potassium (K), and uranium (eU)—providing valuable lithological and alteration mapping capabilities.

Globally, integrated use of aeromagnetic and radiometric datasets has proven effective in identifying geological structures and hydrothermal alteration zones.

For example, Youssef and Elkhodary (2023) used airborne gamma-ray spectrometry to map lithological units in southeastern Aswan City, Egypt, while Wemegah et al. (2022) combined both datasets to interpret the structural framework of the Kumasi Basin. In Nigeria, Adepelumi and Falade (2018) demonstrated their application in uranium exploration, and Aliyu et al. (2021) characterized radioelement concentrations through ground-based radiometric surveys in part of Dutse—though their coverage was geographically limited.

Building on these precedents, this study seeks to assess the geophysical potential of radioelement-hosting minerals in Gaya and its surrounding areas. By integrating aeromagnetic and aeroradiometric datasets, the research aims to produce a comprehensive structural and radiometric interpretation, thereby contributing to informed mineral exploration and resource management in the region.

A. Location and Geology of the Study Area

The study area is situated in the north-western part of Nigeria, between longitudes 11°30'0"N to 12°0'0"N and latitudes 9°0'0"E to 9°30'0"E, encompassing parts of Kano and Jigawa States, including the Local Government Areas of Gaya, Dutse, Ringim, Jahun, Birnin Kudu, and Kiyawa (Figure 1). According to Coker et al. (2020), the area is known for the presence of rocks from the Younger Granites series, which are Jurassic in age, alongside volcanic formations, and occasional younger dykes and flows. The Basement Complex rocks in the region consist of Mesozoic Younger Granite and Pan-African Older Granite formation

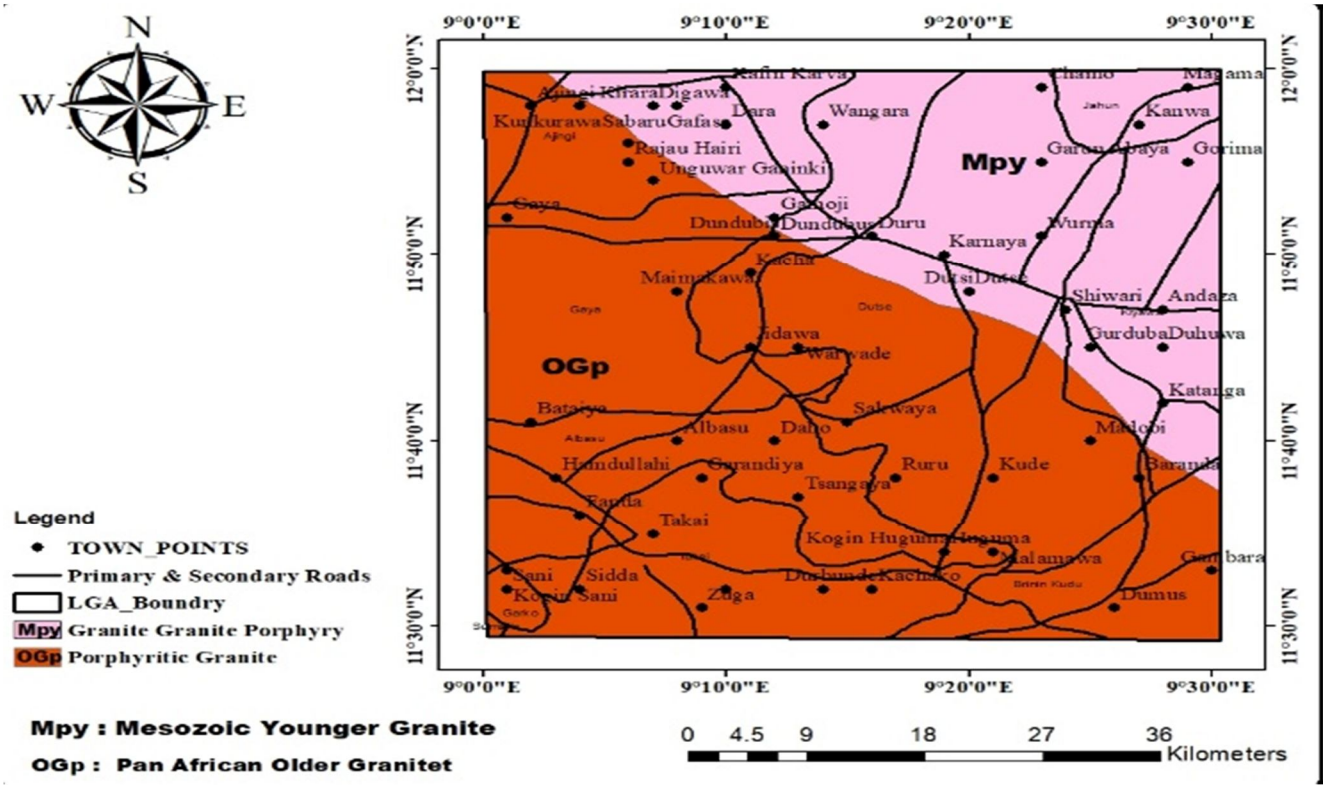

Figure 1a: Geology map of the study area (NGSA (2004), modified on ArcGIS).

II. THEORY OF METHOD ANALYSIS

A. Magnetic Method

A set of mathematical algorithms used to enhance the data for appropriate interpretation is as follows:

1) First Vertical Derivatives (FVD)

The first vertical derivative (FVD) is an enhancement technique that polishes up anomalies over bodies and has a tendency to shrink anomaly complication, in this manner letting clear imaging of the causative structures. The transformation can be noisy meanwhile it will intensify short-wavelength noise, that is, obviously define areas of dissimilar data resolution in the magnetic grid (Kearey *et al*, 2002)

$$FVD = -\frac{\partial M}{\partial z} \quad (1)$$

2) Analytical Signal Amplitude

The analytical technique provides the amplitude response of an anomaly, and also used to identify the boundaries of different geological features.(Debeglia & Corpel, 2012)

$$A(x,y,z) = \sqrt{\left(\frac{\partial M}{\partial x}\right)^2 + \left(\frac{\partial M}{\partial y}\right)^2 + \left(\frac{\partial M}{\partial z}\right)^2} \quad (2)$$

Where A(x, y, z) is the amplitude of the analytical signal at (x, y, z) and M is the observed magnetic anomaly at (x, y, z).

3) Source Parameter Imaging (SPI)

SPI is a technique based on the extension of complex analytic signal (AS) to estimate magnetic depths; it is also known as local wavenumber. The original SPI method works for two models: a 2-D sloping contact or a 2-D dipping thin sheet. For the magnetic field T, the local wavenumber is given by (Telford *et al*., 2012)

$$K(x,y) = \frac{\frac{\partial^2 T}{\partial x\,\partial z}\left(\frac{\partial T}{\partial X}\right) + \frac{\partial^2 T}{\partial y\,\partial z}\left(\frac{\partial T}{\partial X}\right) + \frac{\partial^2 T}{\partial^2 z}\left(\frac{\partial T}{\partial X}\right)}{\left(\frac{\partial T}{\partial x}\right)^2 + \left(\frac{\partial T}{\partial y}\right)^2 + \left(\frac{\partial T}{\partial z}\right)^2} \quad (3)$$

For the dipping contact, the maxima of K are located directly over the isolated contact edges and are independent of the magnetic inclination, declination, dip, and strike respectively.

B. Radiometric Method

1) Radiation Exposure Rate

The radiation exposure rate was calculated using the apparent radioelement concentrations of K (%), eU (ppm), and eTh (ppm),(IAEA, 2000) expressed as

Exposure rate ($\mu R\ hr^{-1}$) = 1.505 K (percent) + 0.653 eU (ppm) + 0.287 eTh (ppm), (4)

where, μ is micro, R is Roentgen and hr. is hour

2) Dose Rate

The dose rate was also calculated, given by(IAEA, 2000)

Dose rate ($mSv\ yr^{-1}$) = 0.0833 x exposure rate ($\mu\ R\ hr^{-1}$), (5)

Where m is mili, Sv is Sievert, and yr. is year

III. METHODOLOGY

This study employs aeromagnetic and aeroradiometric datasets for Sheet 82, acquired from an airborne geophysical survey conducted between 2005 and 2009 by Fugro Airborne Survey Ltd. on behalf of the Nigerian Geological Survey Agency (NGSA).Magnetic field intensity measurements were obtained using a Scintrex CS-3 cesium vapor magnetometer, while gamma-ray spectrometric measurements were collected with a high-sensitivity, 256-channel airborne gamma-ray spectrometer system. The survey was conducted with the following flight specifications:

1) Flight line spacing: 0.5 km
2) Tie line spacing: 2 km
3) Flight line orientation: Northwest–Southeast (NW–SE)
4) Tie line orientation: Northeast–Southwest (NE–SW)
5) Terrain clearance: 80 m

The study area is geographically bounded by longitudes 11°30′0″E to 12°0′0″E and latitudes 9°0′0″N to 9°30′0″N.

A. Data Acquisition

The research integrates both geophysical and geological datasets. The primary geophysical datasets consist of aeromagnetic and aeroradiometric data for Gaya (Sheet 82), while the geological dataset comprises a detailed geological map of the area. All datasets were sourced from the Nigerian Geological Survey Agency (NGSA).

B. Data Processing and Analysis

The study involved several stages of geophysical data processing and interpretation using Oasis Montaj and ArcGIS software. The methodological approach followed established aeromagnetic and radiometric data processing standards to ensure accuracy and geological relevance.

1) Aeromagnetic Data Processing

The aeromagnetic dataset was obtained as total magnetic intensity (TMI) grids with a cell size of 100 m. The first step was the Reduction to the Pole (RTP) transformation, which eliminates the asymmetry in magnetic anomalies by repositioning them directly over their causative bodies (Baranov, 1957; Li, 2008). For this study, the RTP used a magnetic inclination of 1.78° and a declination of −1.05°.

To enhance structural interpretations, the Centre for Exploration Targeting (CET) Grid Analysis was applied to the RTP data. This approach detects structural complexity by identifying lineaments, faults, and intersection zones indicative of mineralization (Holden et al., 2008). Noise and background effects were minimized using amplitude thresholding, and standard deviation filters were applied to estimate magnetic variation symmetry and isolate continuous magnetic trends (Fairhead et al., 2004).

For additional subsurface characterization, the Analytic Signal method (MacLeod et al., 1993) and the Tilt-Depth Method (Salem et al., 2014) were used to estimate depths to magnetic sources and enhance weak anomaly signatures.

2) Aeroradiometric Data Processing

The airborne radiometric data consisted of potassium (K), equivalent thorium (eTh), and equivalent uranium (eU) grids. These datasets were corrected and processed following the IAEA guidelines for radioelement mapping (IAEA, 2003; Grasty & Minty, 1995). The interpretation incorporated geochemical relationships between radioelements to infer lithology and alteration zones (Dickson & Scott, 1997; Wilford et al., 1997).

A K/eTh ratio map was generated to highlight potential hydrothermal alteration zones, as elevated K relative to eTh can indicate potassium enrichment associated with mineralization (Ostrovskiy, 2011). Additionally, a ternary RGB map was created, with K, eTh, and eU assigned to the red, green, and blue channels respectively, to facilitate lithological discrimination and radiometric pattern recognition (Youssef & Elkhodary, 2023).The diagram Figure 3 outlines the sequential steps from geophysical data acquisition to aeromagnetic and radiometric processing, culminating in the integration of results for structural, lithological, and alteration zone mapping.

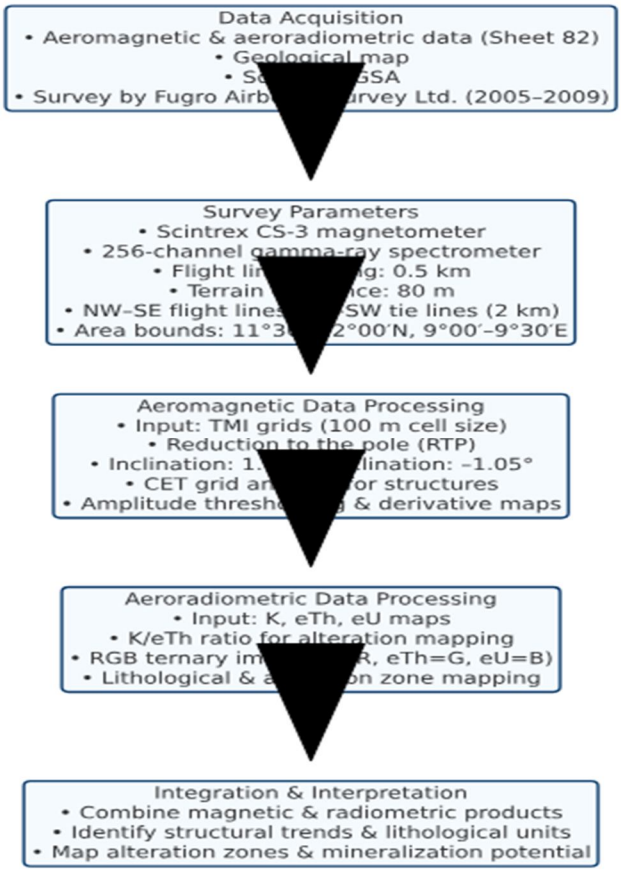

Figure 1b. *Workflow of data acquisition, processing, and interpretation.*

IV. RESULTS AND DISCUSSION

In this study different application techniques of data analysis and interpretation have been produced many results using the acquired aeromagnetic and aeroradiometric data.

A. Results

The captured coordinates values of longitudes and latitudes, location and direction of residual, source parameter imaging, and ternary maps, revealed that the relative correlation associated with rock units as shown in the table1

Table 1: Point of Anomalies, Depth and Radioactive Zones Captured from Residual, SPI, and Ternary maps

Rock Units	Residual Anomaly	SPI map	Ternary map	Longitude Meter (m) Min	Longitude Meter (m) Max	Latitude Meter (m) Min	Latitude Meter(m) Max	Location	Direction
Myp	a	SD(0.26 -0.7km)	HC(eU)	5.46	5.54	13.16	13.23	Kanwa	NE
-	b	-	HC(eU,K)	5.39	5.43	13.14	13.18	Karnaya	-
-	c	-	HLC,eU,K	5.33	5.38	13.09	13.13	Garun Abaya	-
-	d	-	HC(eU)	5.45	5.50	12.96	13.02	Dutsi Dutse	NE
-	e	-	H(eU,K)	5.41	5.44	13.07	13.11	Gurduba	-
-	f	-	-	5.40	5.53	13.03	13.07	Shiwari	NE
OGp	g	DD(0.08 -0.2km)	HC(eU,K, eTh)	5.38	5.46	12.83	12.88	Kude	SE
Myp	h	SD(0.26 -0.7km)	HC(eU)	5.44	5.51	13.11	13.14	Wurnoma	NE
OGp	i	DD(0.08 -0.2km)	HLC	5.40	5.54	12.84	12.85	Baranda	SW
-	j	SD(0.26 -0,7km)	HC(eTh)	5.03	5.07	13.13	13.16	Gaya	NW
-	k	-	HCL	5.06	5.09	12.88	12.80	Hamdullahi	SW

Mesozoic Younger granite: (Myp), Pan Africa Older granite: (OGp) Anomaly: (a-k), Shallow Depth :(SD), Deep Depth :(DD) High :(H), High concentration Level: (HCL), High Content of Potassium, Thorium &Uranium: HC (K, eTh, eU), Northeast (NE), Northwest :(NW), Southeast :(SE), Southwest :(SW)

The statistical calculation of air gamma ray spectrometer showing variables of radioelements with Mean(X), Standard deviation (STD) and Coefficient of Variation (CV) as shown in table 2

Table 2. Statistics of the airborne gamma-ray spectrometric data for all rock units with respect to Gaya and its environs.

Variables	Minimum	Maximum	Range	Mean (X)	Standard deviation STD	Coefficient of variation (CV %)
TC (Ur)	11.31	29.21	17.9	15.93	4.34	27.24
K (per cent)	0.19	4.24	4.43	0.7	0.36	51.42
eU (ppm)	1.34	4.65	3.27	2.79	0.66	23.66
eTh (ppm)	8.07	23.44	15.37	12.13	3.44	28.36
eU/eTh	0.13	0.37	0.24	0.24	0.04	16.67
eU/K	1.05	6.57	5.52	2.95	0.90	30.51
Dose ($nGyph^{-1}$)	0.97	464.33	463.36	47.09	17.04	36.19

The statistical dose rate computed the Mean(X) and Standard deviation (STD) in mili Sievert per year associated with each rock unit as shown in table3.

Table 3: Dose rate in $mSvyr^{-1}$ for each Rock Unit for Gaya and its environs

Rock Unit	Dose rate ($mSvyr^{-1}$)		Mean (X)	Standard Deviation (STD)
	Minimum	Maximum		
Myp(a)	0.30	0.66	0.40	0.11
Myp(b)	0.30	0.39	0.34	0.02
Myp(c)	0.26	0.51	0.33	0.05
Myp(d)	0.24	0.54	0.32	0.06
Myp(e)	0.32	0.38	0.34	0.01
OGp(f)	0.39	0.77	0.48	0.11
OGp(g)	0.39	1.01	0.59	0.14
OGp(h)	0.38	1.01	0.53	0.13
OGp(i)	0.33	0.52	0.42	0.03
OGp(j)	0.11	1.01	0.53	0.18

Mesozoic Younger Granite (Myp), Pan African Older Granite (OGp)

Figure 2 illustrates the range of Total Magnetic Intensity (TMI) values recorded in the study area, which span from a minimum of 33,724.9 nanoteslas (nT) to a maximum of 34,179 nT. This variation in TMI values suggests the presence of diverse magnetic features within the subsurface, which could be related to different geological structures, such as magnetic anomalies, fault zones, or mineralized bodies. These values provide valuable insights into the magnetic properties of the underlying rocks and their potential to host various geological formations, which will aid in further interpretation of the area's geophysical characteristics. The data serves as a foundation for identifying key structural features and guiding further exploration in the region.

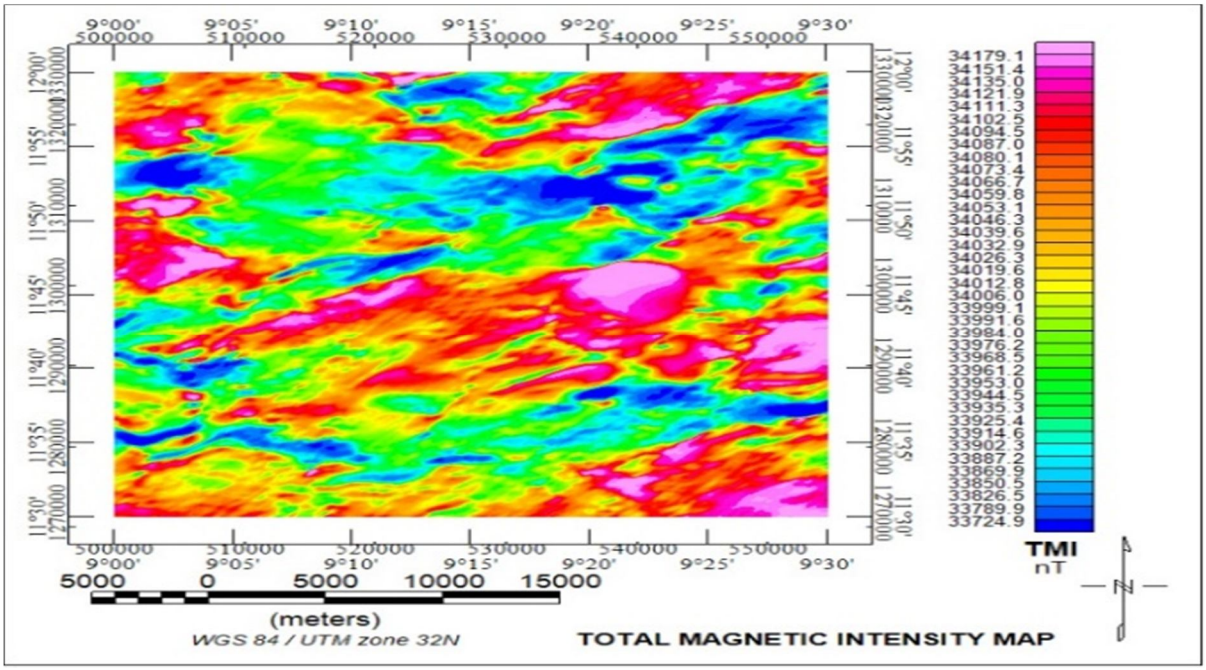

Figure 2: Total Magnetic Intensity Map of the Study Area

The Figure 3 revealed that the residual magnetic field intensity map showed anomaly value from low to high and ranged from -293.1nT to 436.1nT. This indicates that the study area is characterized by low (blue color) and high (pink color) magnetic signatures. Generally, the entire study area revealed positive and negative residual anomalies, indicating the sequence of magnetic highs and lows. Figure 4 shows that the Analytic Signal Amplitude (ASA) of the study area was obtained from residual magnetic data. The ASA shows the amplitude contrast of the crustal rocks and structures varying from 0.031 nT/m to 0.592 nT/m areas with pink and red colors.

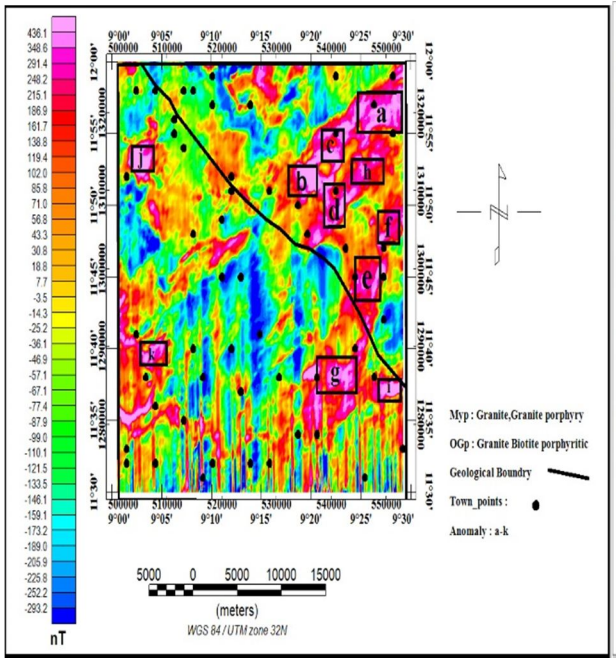

Figure 3 Residual Map of the Study Area

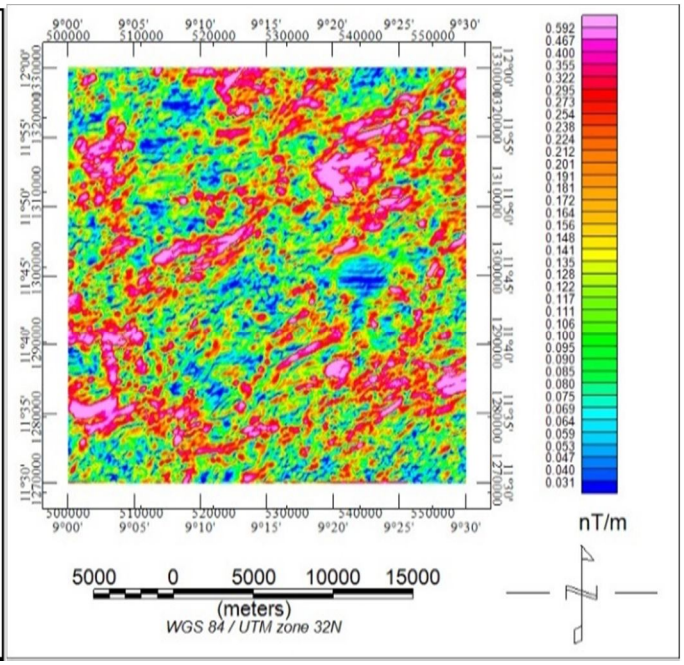

Figure 4: Analytical signal Map of the Study Area

Figure 5 reveals structural anomalies predominantly trending in the NE-SW direction, suggesting a strong correlation with weathered granite intrusions underlying the study area. Regions exhibiting low positive structural anomalies are associated with sedimentary formations. Furthermore, the lineament map in Figure 6 indicates structural trends consistent with those observed in the first vertical derivative analysis. These lineaments likely represent geological features such as fractures, faults, joints, and dykes, which may serve as potential hosts for mineralization, particularly radioactive elements, within the study area.

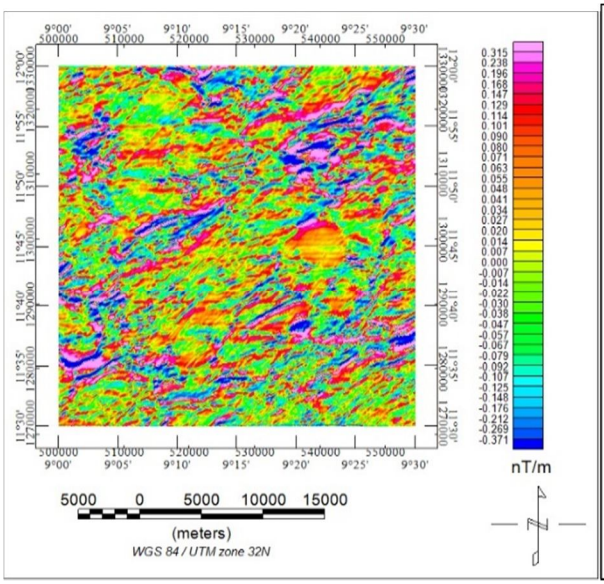

Figure 5: FVD Map of the Study Area

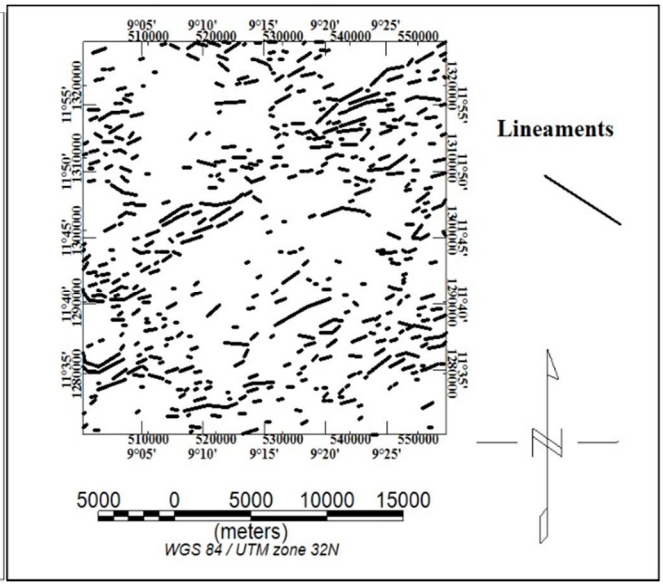

Figure 6: Lineament Map of the Study Area

The Figure 7 revealed two different depth sources; shallow depth and deeper depth. The areas with blue colour depict the shallow depth and the areas with pink color depict the deeper depth. Therefore both shallow and deep depth sources are interested which could be suspected that accommodate the occurrence of radioelements mineral potential zones. The shallow depth source ranges from 0.08km to 0.201km, and the area more prominent at the South East (SE) and the deeper depth source ranges from 0.261 km to 0.7979 km and predominantly trended from NE-NW and SW direction respectively.

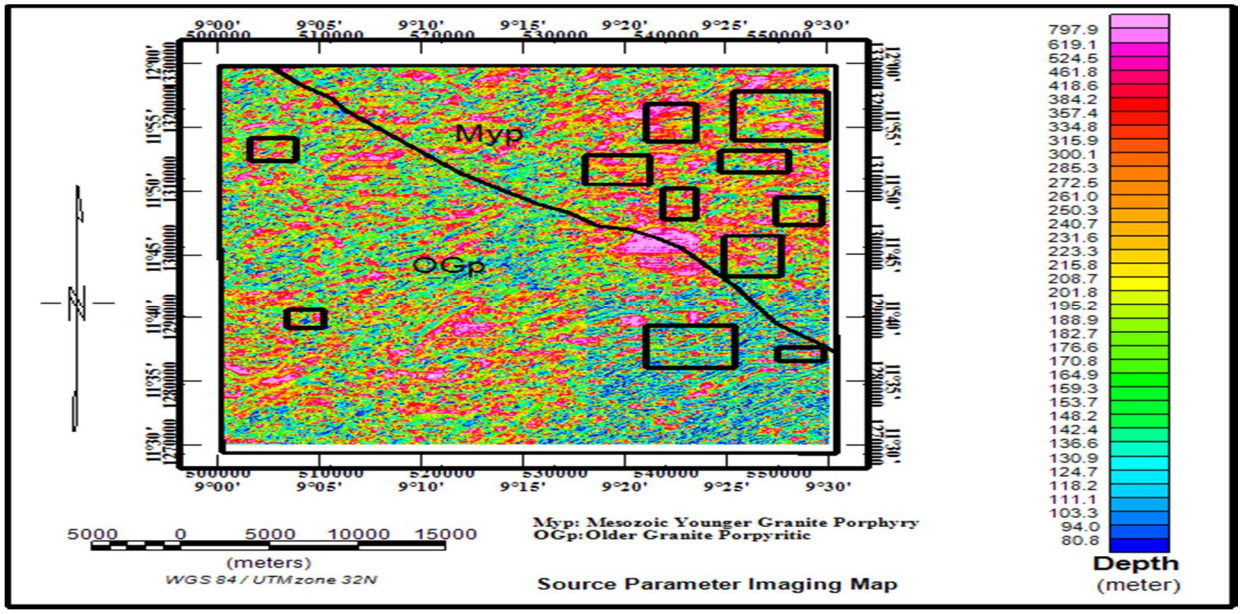

Figure 7: SPI Map of the Study Area

The potassium Figure 8 indicated that (K%) is concentrated in the southwestern and south-eastern parts trending in an east-west direction and the high concentration value of potassium (pink color) is indicated as 1.8%, and the low concentration value (blue color) signified as 0.3%.

Figure 9 displayed the concentration of thorium is low around, the northeast part of the study area, thorium is highly concentrated in the SW, SE and NE direction. The high concentration value is 19.5ppm indicated as pink color while the low concentration value is 6.1ppm indicated as blue color. Figure 10 displayed the concentration of uranium trended from NW, E-W, and SS direction parts of the study area, the high concentration value is 4.3ppm indicated as pink color and the low concentration value is 1.3ppm signified as blue color.

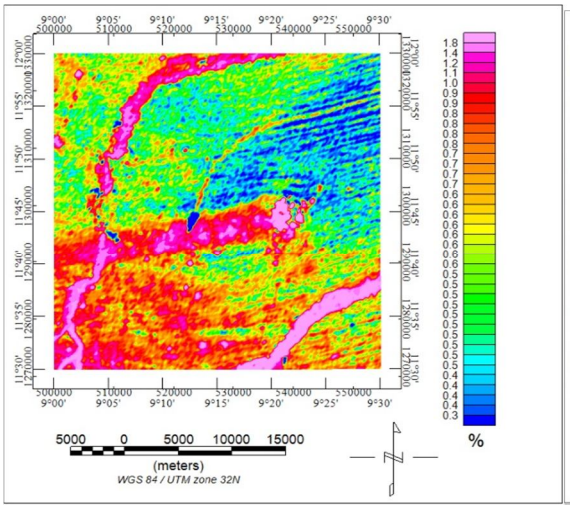

Figure 8; Potassium Map of the Study Area

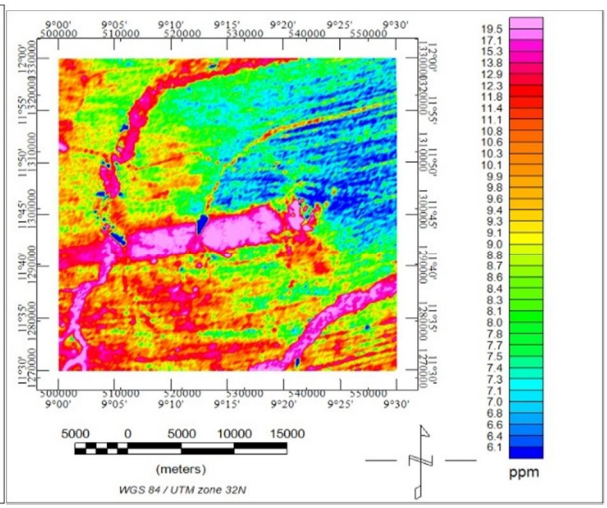

Figure 9: Thorium Map of the Study Area

The eU/eTh ratio, which is important in uranium exploration, depends mainly on the mobile elements (i.e., uranium), and it also determines uranium enrichment areas. According to, the eU/eTh ratio for granitic rock is about 0.33; the enrichment area is above 0.33 in granites, while leaching out of uranium will be indicated by its decrease to less than 0.3. From the eU/eTh ratio map Figure 11, most of the granitic rocks in the study area have relatively low values.

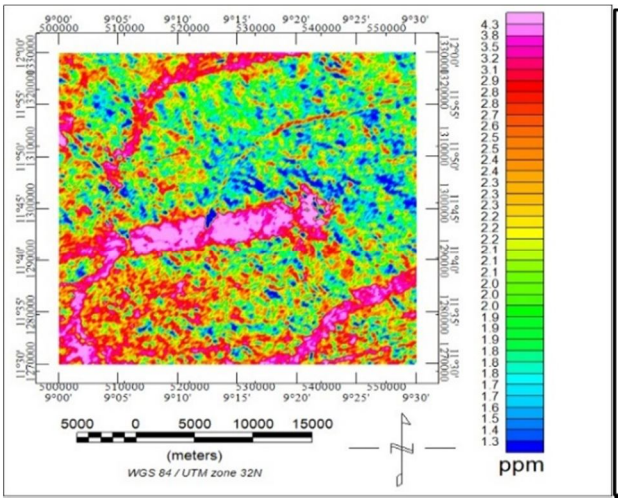

Figure 10: Uranium Map of the Study Area

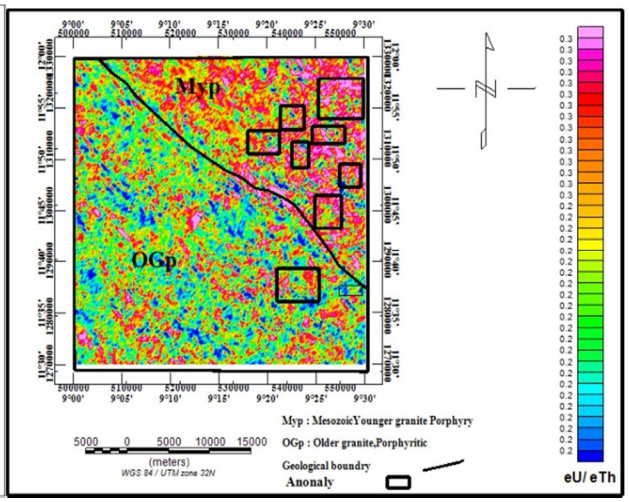

Figure 11: eU/eTh Map of the Study Area

Figure 12 presents the ternary composite image map of the study area, generated from gamma-ray spectrometric data representing the concentrations of potassium (K%), equivalent uranium (eU), and equivalent thorium (eTh). This map effectively illustrates the spatial distribution and variations in the three radioelements, primarily reflecting lithological differences. In the triangular legend, potassium is represented in red, thorium in green, and uranium in blue, with each pure color signifying a 100% concentration of the respective radioelement.

The ternary map reveals that the Younger Granites exhibit high uranium (eU) and potassium (K) concentrations while showing relatively low thorium (eTh) content. Notably, areas with traces of high uranium (blue) but moderate potassium and low thorium concentrations are predominantly observed in the northeastern part of the study area. Conversely, the Older Granites are characterized by elevated thorium (green) levels, with lower uranium and potassium concentrations. Additionally, regions of high radioactive concentration appear as white zones, whereas black zones indicate areas with weak radioactive concentrations. This visualization provides crucial insights into the geochemical variations and potential mineralization zones within the study area.

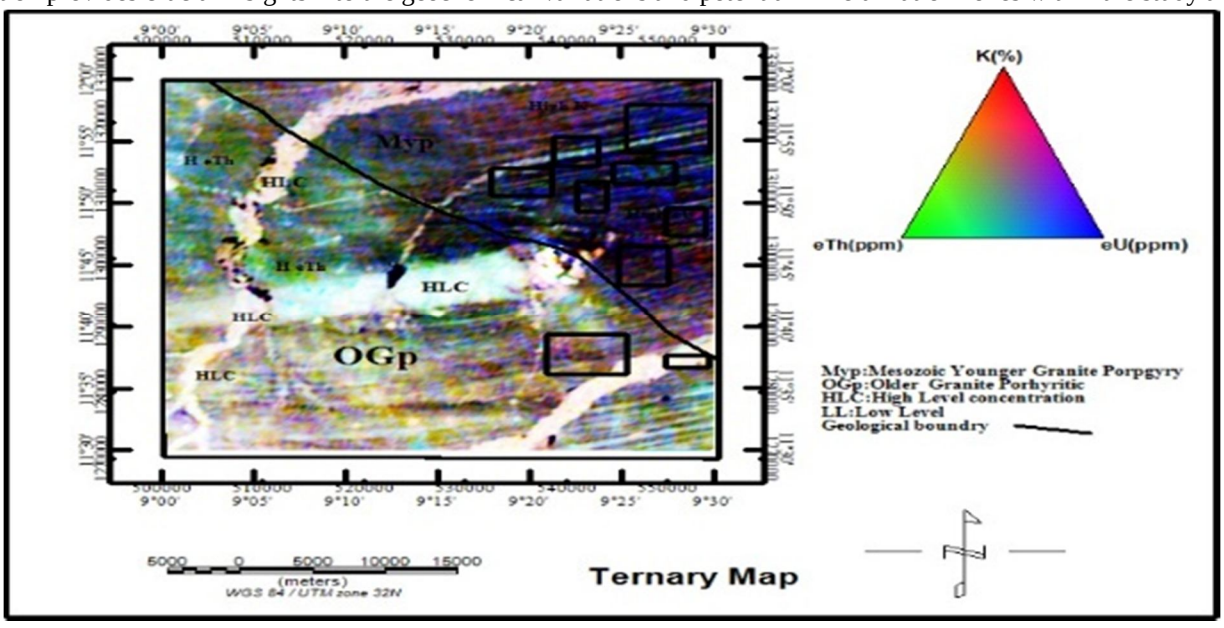

Figure 12: Ternary Map of the Study Area

B. Discussion of the Results

The comprehensive analysis of the figures reveals important geophysical and geological characteristics of the study area, focusing on the spatial distribution of magnetic anomalies, structural features, depths of magnetic sources, and concentrations of radioelements. These findings offer significant insights into lithological variations, mineralization potential, and radioactive element distribution, as well as the interpretation of results from Tables 4.1, 4.2, 4.3, and 4.4.

Table 4.1 correlates residual anomaly and ternary maps with location and rock units, covering geological formations such as Younger Granite (Myp) and Older Granite Porphyry (OGp). The residual anomaly column reflects varying magnetic anomaly degrees across the study area, highlighting areas of potential mineralization or geological significance. The depth categories distinguish shallow anomalies (0.08 to 0.2 km) from deeper anomalies (0.26 to 0.7 km). Shallow anomalies are concentrated in regions like Kanwa, Gurduba, and Wurnoma, while deeper anomalies are observed in Kude and Baranda. The ternary map provides valuable data on Uranium (eU), Thorium (eTh), and Potassium (K) concentrations, helping identify potential ore zones. Locations such as Kanwa and Wurnoma show a northeast (NE) directional trend, aligning with regional geological patterns.

Table 4.2 offers a qualitative analysis of aeroradiometric concentration maps for Uranium, Thorium, and Potassium. Areas like Gafasa and Wangara exhibit high concentrations of Uranium (H > 20), Thorium (H > 15.3), and Potassium (H > 1.1), suggesting significant mineral concentrations. Conversely, locations like Gorima and Shiwari show lower concentrations, indicating areas with less mineralization potential.

Table 4.3 presents statistical details of airborne gamma-ray spectrometric data, including Uranium (eU), Thorium (eTh), Potassium (K), and Total Count (TC). The data shows considerable variability, with the total count ranging from 11.31 to 29.21 and a mean of 15.93, indicating significant fluctuations in radioactive element distribution. The eU/eTh and eU/K ratios, ranging from 0.13 to 0.37 and 1.05 to 6.57, suggest variations in Uranium distribution relative to Thorium and Potassium, important for mineral prospecting.

Table 4.4 explores the dose rates for different rock units, with values ranging from 0.11 to 1.01 mSv/yr. Some units, like OGp(g), show higher dose rates, possibly due to elevated radioactive element concentrations. The findings indicate that while the dose rates are within expected geological ranges, higher rates in certain units may warrant further investigation for mineralization and safety assessments.

The magnetic analysis examines total magnetic intensity (TMI), residual magnetic fields, analytic signal amplitude, first vertical derivative, and lineament maps. TMI values range from 33,724.9 nT to 34,179 nT, highlighting variations in the Earth's magnetic field and the magnetic susceptibility of underlying rocks. Residual magnetic anomalies, ranging from −293.1 nT to 436.1 nT, reflect lithological heterogeneity, with positive anomalies indicating magnetically enriched rocks like granites, and negative anomalies signaling weathered zones. The analytic signal amplitude map reveals magnetic contrasts, while the first vertical derivative and lineament maps indicate NE–SW trending structural anomalies, which may correlate with mineralized zones.

The magnetic source depth analysis (Figure 7) shows shallow sources (0.08 km to 0.2 km) primarily concentrated in the southeastern region, indicating potential near-surface mineralization. Deeper sources (0.26 km to 0.8 km) are prevalent in NE–NW and SW trends, likely corresponding to basement structures or intrusive rocks.

In the radiometric analysis, high concentrations of Potassium, Thorium, and Uranium are observed in various regions, such as the SW and SE, indicating mineral-rich zones. The eU/eTh ratio suggests minimal uranium enrichment in granitic rocks, with thorium dominance in certain lithologies. The ternary map further visualizes the spatial distribution of radioelements, identifying Younger Granites (Myp) with potential for uranium-rich deposits, and Older Granites (OGp) with thorium as the dominant radioactive element.

The dose rate in the study area ranges from 0.97 nGy h^{-1} to 464.33 nGy h^{-1}, with an average of 47.09 nGy h^{-1}, closely aligning with Aliyu (2020), who reported values ranging from 33.45 nGy h^{-1} to 676.49 nGy h^{-1}, with an average of 48.4 nGy h^{-1}. While Aliyu's study relied on ground radiometric methods, the present study employed an integrated aeromagnetic and aeroradiometric approach. Similar dose rate magnitudes have been reported in other parts of Nigeria. For example, in the Wukari–Donga area of the Middle Benue Trough, mean dose rates of ~40.33 nGy h^{-1} were observed, corresponding to an annual effective dose of ~49.46 µSv y^{-1}, well below UNSCEAR's global outdoor average of 70 µSv y^{-1} (Oladunjoye et al., 2020). In contrast, granite-rich areas like Ilesha have recorded higher annual effective doses ranging from 0.18 to 3.93 mSv y^{-1}, still within geological norms (Ogunyele et al., 2018).

Comparable aeroradiometric investigations in North-Central Nigeria identified high K/eTh ratios associated with hydrothermal alteration zones and structural lineaments (Akinyemi et al., 2021). This supports the present study's interpretation that NE–SW structural trends may act as pathways for mineralizing fluids.

According to IAEA (2000) safety guidelines, occupational exposure thresholds are around 1 mSv y^{-1} (≈0.5 µSv h^{-1} over a working year), and the dose levels in the study area (~0.047 µSv h^{-1}) remain far below these limits.

The global average annual exposure to natural sources is ~2.4 mSv y^{-1} (UNSCEAR, 2000), with the terrestrial gamma component contributing ~0.48 mSv y^{-1}. Therefore, the radiological exposure in this region can be considered minimal, with negligible health risks, while the integrated geophysical data indicate significant mineralization potential in specific lithological units.

V. CONCLUSIONS

This study has demonstrated the effectiveness of integrating aeromagnetic and radiometric methods in delineating mineralization zones within the study area. The identified NE–SW and NW–SE structural trends, shallow magnetic source depths (0.08–0.20 km), and elevated uranium (up to 8.26 ppm), thorium (up to 35.47 ppm), and potassium (up to 3.96%) concentrations point to significant exploration potential. Key target zones, including Kanwa, Gurduba, and Wurnoma, display geophysical and geochemical characteristics consistent with mineralized systems.

The measured average radiological dose rate (47.09 nGy h^{-1}) remains well below international safety limits, suggesting minimal environmental health risks. The correlation of current findings with previous regional surveys provides additional confidence in the interpretive results and confirms the structural and lithological controls on mineralization. Overall, the study offers a robust geophysical framework for guiding targeted mineral exploration while ensuring adherence to radiological safety standards.

REFERENCES

[1] Adepelumi, A. A., & Falade, A. H. (2017). Combined high-resolution aeromagnetic and radiometric mapping of uranium mineralization and tectonic settings in Northeastern Nigeria. Acta Geophysica. https://doi.org/10.1007/s11600-017-0080-3
[2] Aliyu, A., Wada, A., Ahmad, A., & Muhammad, D. (2021). Investigation of an Aerospectrometric Anomaly Using Ground Gamma Ray Spectrometry Sheet 81, Dutse North-Western Nigeria. Science Forum (Journal of Pure and Applied Sciences), 20(1), 1. https://doi.org/10.5455/sf.58915
[3] Akinyemi, O., Falode, A., & Bello, R. (2021). Aeromagnetic and aeroradiometric mapping of hydrothermal alteration zones in North-Central Nigeria. International Journal of Geophysics and Geochemistry, **12**(3), 110–125.
[4] Baranov, V. (1957). A new method for interpretation of aeromagnetic maps: Pseudo-gravimetric anomalies. Geophysics, 22(2), 359–383. https://doi.org/10.1190/1.1438369
[5] Coker, J. O., Agbelemoge, A. J., Ariyo, S. O., Makinde, V., Alabi, A. A., & Emida, A. A. (2020). Investigation of Groundwater Potentials in Imakun Omi Community Using Electrical Resistivity Method. African Journal of Science and Nature, 7, 19. https://doi.org/10.46881/ajsn.v7i0.153
[6] Debeglia, N., & Corpel, J. (2012). Automatic 3-D interpretation of potential field data using analytic signal derivatives. Geophysics, 62(1), 87–96. https://doi.org/10.1190/1.1444149
[7] Eldosouky, A. M., Abdelkareem, M., & Elkhateeb, S. O. (2017). Integration of remote sensing and aeromagnetic data for mapping structural features and hydrothermal alteration zones in Wadi Allaqi area, South Eastern Desert of Egypt. Journal of African Earth Sciences, 130, 28–37. https://doi.org/10.1016/j.jafrearsci.2017.03.006
[8] Elkhateeb, S. O., & Abdellatif, M. A. G. (2018). Delineation potential gold mineralization zones in a part of Central Eastern Desert, Egypt using Airborne Magnetic and Radiometric data. NRIAG Journal of Astronomy and Geophysics, 7(2), 361–376. https://doi.org/10.1016/j.nrjag.2018.05.010
[9] Fairhead, J. D., Green, C. M., Verduzco, B., & Mackenzie, C. (2004). A new set of magnetic field derivatives for mapping mineral prospects. The Leading Edge, 23(4), 278–283. https://doi.org/10.1190/1.1705542
[10] Grasty, R. L. (2009). Gamma Ray Spectrometric Methods In Uranium Exploration - Theory And Operational Procedures R.L. Grasty Geological Survey of Canada, Ottawa. 1910.
[11] Grasty, R. L., & Minty, B. R. S. (1995). A guide to the technical specifications for airborne gamma-ray surveys. AGSO Journal of Australian Geology & Geophysics, 16(2), 187–194.
[12] Holden, E. J., Dentith, M., & Kovesi, P. (2008). Towards the automatic analysis of regional aeromagnetic data to identify regions prospective for gold deposits. Computers and Geosciences, 34(11), 1505–1513
[13] Kearey, P., Brooks, M. & Hill, I. (2002). An Introduction to Geophysical Exploration. 3rd Edition, Blackwell Science ltd, Malden Mass.
[14] Lenntech (2023). Chemical Properties and Applications of Uranium. Retrieved from http://www.lenntech.com/index.htm on 11/09/2013
[15] IAEA. (2000). Uranium exploration data and techniques applied to the preparation of radioelement maps. May, 440.
[16] MacLeod, I. N., Jones, K., & Dai, T. F. (1993). 3-D analytic signal in the interpretation of total magnetic field data at low magnetic latitudes. Exploration Geophysics, 24(4), 679–688. https://doi.org/10.1071/EG993679
[17] NGSA (2023). Geological map of Nigeria. A compilation by Nigerian Geological Survey Agency, 20023 Edition.
[18] Oladunjoye, O., Akande, S., & Ojo, J. (2020). Natural gamma dose rates and environmental radiation levels in the Wukari-Donga area, Nigeria. Journal of Environmental Radioactivity, **223**, 106362.
[19] Ogunyele, B., Akinlabi, A., & Oladunjoye, O. (2018). Radiological characterization of granite-rich zones in Ilesha, southwestern Nigeria. Environmental Earth Sciences, **77**(5), 152.
[20] Ostrovskiy, E. A. (2011). Antagonism of radioactive elements in wallrock alteration fields and its use in aero-gamma spectrometric prospecting. International Geologiy Review, 17(4), 461–468.
[21] Plant, J. A., Reeder, S., Salminen, R., Smith, D. B., Tarvainen, T., De Vivo, B., & Petterson, M. G. (2003). The distribution of uranium over Europe: Geological and environmental significance. Transactions of the Institution of Mining and Metallurgy, Section B: Applied Earth Science, 112(3), 221–238. https://doi.org/10.1179/037174503225003152
[22] Salem, A., Williams, S., Fairhead, J. D., Ravat, D., & Smith, R. (2014). Tilt-depth method: A simple depth estimation method using first-order magnetic derivatives. The Leading Edge, 33(12), 1428–1434. https://doi.org/10.1190/tle33121428.1

[23] Telford, W. M., Geldart, L. P., & Sheriff, R. E. (2012). Magnetic Methods. In Applied Geophysics. https://doi.org/10.1017/cbo9781139167932.007
[24] Tukel A. K, Y. and Kahriman, A. (2009). Importance of Thorium as an Alternative Energy Source and the Role of Turkey. 9th International Multidisciplinary Scientific GeoConference. SGEM 2009]
[25] UMMC (2013). Importance of potassium. Retrieved from University of Maryland Medical Centre (UMMC): website: http://medschool.umaryland.edu
[26] UNSCEAR. (2000). Sources and Effects of Ionizing Radiation. United Nations Scientific Committee on the Effects of Atomic Radiation.
[27] Wemegah, D. D., Preko, K., Noye, R. M., Boadi, B., Menyeh, A., Danuor, S. K., & Amenyoh, T. (2015). Geophysical Interpretation of Possible Gold Mineralization Zones in Kyerano, South-Western Ghana Using Aeromagnetic and Radiometric Datasets. Journal of Geoscience and Environment Protection, 03(04), 67–82. https://doi.org/10.4236/gep.2015.34008
[28] Youssef, M. M., & Elkhodary, S. M. (2023). Application of airborne gamma-ray spectrometric data for lithological mapping in southeastern Aswan City, Egypt. Journal of African Earth Sciences, 203, 104941. https://doi.org/10.1016/j.jafrearsci.2023.104941

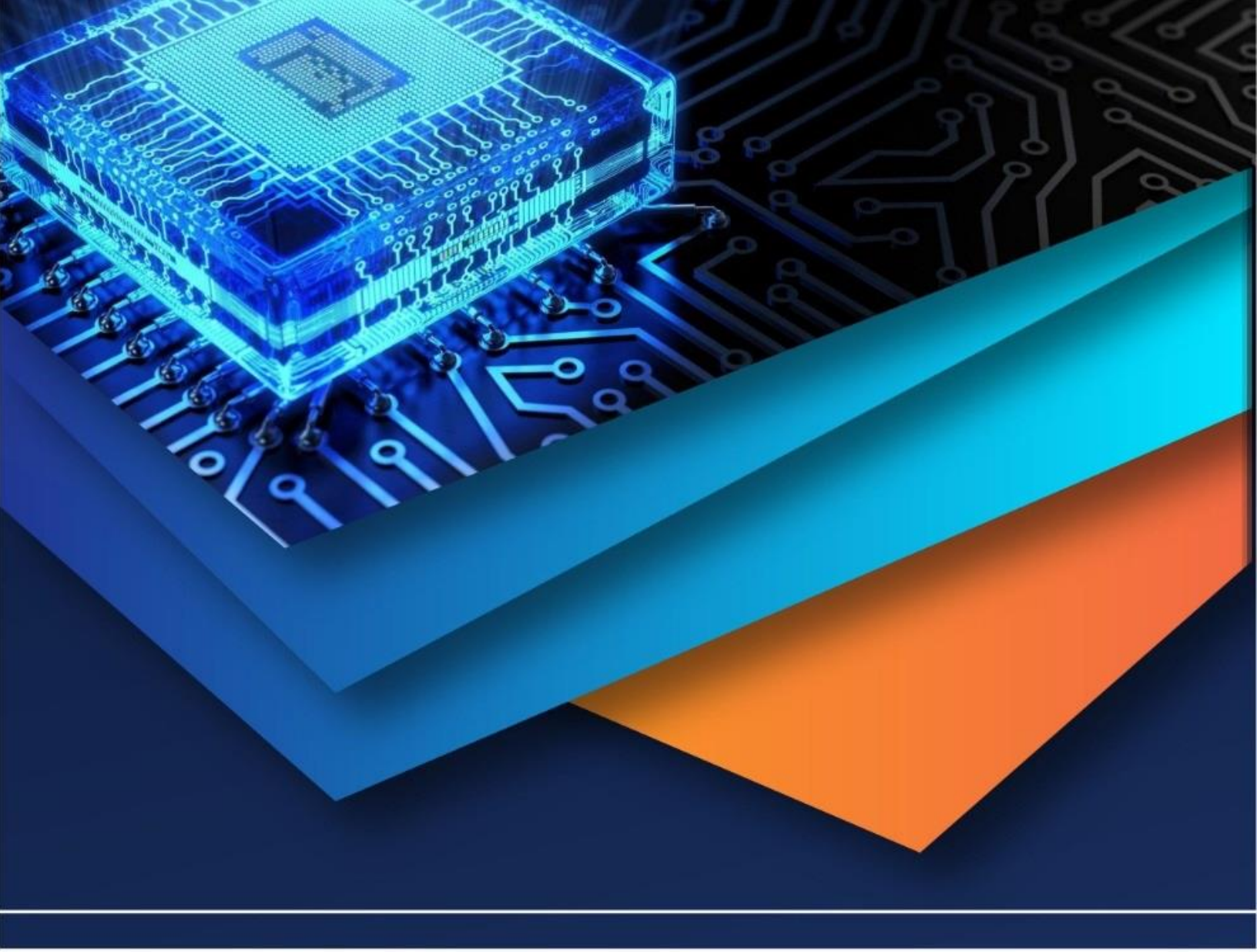

10.22214/IJRASET

45.98

IMPACT FACTOR: 7.129

IMPACT FACTOR: 7.429

INTERNATIONAL JOURNAL FOR RESEARCH

IN APPLIED SCIENCE & ENGINEERING TECHNOLOGY